

On consistent parameterizations for both dominant wind-waves and spectral tail directionality

Matias Alday^{1,2}, and Fabrice Ardhuin²

¹Marine Renewable Energies Lab., Department of Hydraulic Engineering, Delft University of Technology,
Delft, The Netherlands

²Univ. Brest, CNRS, Ifremer, IRD, Laboratoire d'Océanographie Physique et Spatiale, Brest, France

Key Points:

- A spectral wave model is adjusted to produce accurate properties for both dominant and short waves
- A balance between 4-wave non-linear interactions and dissipation can explain directional bimodality
- Dissipation must be very weak for waves travelling at 90 degrees and more from the wind direction

Corresponding author: Matias Alday, M.F.AldayGonzalez@tudelft.nl, malday@ifremer.fr

Abstract

Numerical wave models have been developed to reproduce the evolution of waves generated in all directions and over a wide range of wavelengths. The amount of wave energy in the different directions and wavelength is the result of a number of physical processes that are not well understood and that may not be represented in parameterizations. Models have generally been tuned to reproduce dominant wave properties: significant wave height, mean direction, dominant wavelengths. A recent update in wave dissipation parameterizations has shown that it can produce realistic energy levels and directional distribution for shorter waves too. Here we show that this new formulation of the wave energy sink can reproduce the variability of measured infrasound power below a frequency of 2 Hz, associated with a large energy level of waves propagating perpendicular to the wind, for waves with frequencies up to at least 1 Hz. The details are sensitive to the balance between the non-linear transfer of energy away from the wind direction, and the influence of dominant and relatively long waves on the dissipation of shorter waves in other directions.

Plain Language Summary

As the wind blows over the ocean, waves are generated in all directions and over a wide range of wavelengths. The amount of wave energy in the different directions and wavelength is the result of a number of physical processes that are not well understood. Practical models used for marine weather and engineering use a decomposition of the wave field across all these different directions and wavelengths. The sources and sinks of energy of the different components have usually been adjusted to properly represent the total energy, the dominant wavelengths and mean directions, with generally bad results for the shorter wave energy and its directional distribution. Here we show that a recently proposed formulation for the energy sink can be adapted to produce realistic levels of short wave energy in all directions, revealing the importance of different evolution time scales for different wave components. Our wave model is validated using a wide range of measurements, including underwater infrasound power that is related to the presence of waves in opposing directions.

Keywords: Wave dissipation, nonlinear interactions, spectral shape, source term balance, WAVEWATCH III

1 Introduction

Parameterizations in numerical models are generally introduced to describe processes that cannot be explicitly represented because they are not fully understood or would require a computational power that is not available. For ocean and atmosphere circulation models this is particularly the case for small scale processes related to sub-grid motions. In wave models, the sea state is described by the power spectral density of the surface elevation $E(f, \theta)$, distributed across frequency f and direction θ , and parameterizations are mostly used in the representation of the spectral evolution source term $S(f, \theta)$ on the right hand side of the wave energy balance equation (Komen et al., 1994). These parameterizations are necessary because of either poorly understood physical processes, in particular for the source term $S_{\text{in}}(f, \theta)$ that represents the generation of waves by the wind (Miles, 1957; Janssen, 1991) and the dissipation source term $S_{\text{ds}}(f, \theta)$ that accounts for wave breaking (Phillips, 1985), or processes for which the accurate theoretical source term takes a form that is too costly to evaluate at each model time step. The latter is the case of the non-linear 4-wave interaction source term $S_{\text{nl}}(f, \theta)$ (Hasselmann, 1962), for which the Discrete Interaction Approximation (DIA) of Hasselmann et al. (1985) is the parameterization used in most application cases and it simplifies the interaction for each spectral component as the interaction within only two sets of 4 interacting wave

components, known as quadruplets, instead of a the integration over many more quadruplets, possibly thousands of them.

The general difficulty of wave modelling is that the model uses a spectral dissipation rate $S_{ds}(f, \theta)$ that is not measured directly. Here we will particularly discuss the impact of the spectral shape of S_{ds} on the shape of the wave spectrum $E(f, \theta)$ and several parameters that can be measured and can be defined from the spectrum. One of these parameters is the directional spread, which is accessible from buoy measurements for frequencies up to 0.4 Hz (O'Reilly et al., 1996), and of particular interest is the so-called “overlap integral” $I(f)$, which is only a function of the directional distribution of wave energy $M(f, \theta) = E(f, \theta)/E(f)$, with

$$E(f) = \int_0^{2\pi} E(f, \theta) d\theta, \quad (1)$$

and

$$I(f) = \int_0^{2\pi} M(f, \theta) M(f, \theta + \pi) d\theta. \quad (2)$$

Indeed underwater acoustic measurements at frequencies $f_s = 2f$ with f in the range 0.1 to 10 Hz, are expected to be proportional to the value of $E(f)^2 I(f)$ (Farrell & Munk, 2010), while $E(f)$ at those frequencies has a limited range of variation (Elfouhaily et al., 1997; Yurovskaya et al., 2013). Hence underwater acoustics open a unique window on wave frequencies over 0.4 Hz for which very little spectrally resolved data is available.

In the present paper we particularly focus on the form of the dissipation term associated to wave breaking. Our starting point in section 2 is a description of the parameterization proposed by Romero (2019), who introduced unique features that make it possible to reproduce the directional distribution of waves with frequencies higher than twice the wind sea peak frequency. We also present possible adjustments that may be needed to fit a wide range of observations. In section 3 we look at the global-scale performance of this parameterization using usual satellite altimeter and buoy data that provide a measure of the dominant waves, and underwater acoustic measurements that provides some control of the directionality in the spectrum tail. Discussions and conclusions follow in section 4.

2 Dissipation parameterization and impact on spectral shape

At very high frequencies, the dissipation caused by molecular viscosity that scales like the wavenumber squared should be important, together with the straining of turbulence by the Stokes drift shear that scales like the wavenumber to the power 1.5 (Ardhuin & Jenkins, 2006). These are particularly relevant for gravity-capillary waves (Dulov & Kosnik, 2009), and certainly contribute to the shape of the full spectrum (Elfouhaily et al., 1997), with an indirect effect on the dominant waves via the wind stress (Janssen, 1991). However, as we limit our investigation to a maximum frequency of 1 Hz, we will neglect these effects and the dissipation is expected to be controlled by wave breaking (Sutherland & Melville, 2013).

With very limited information on the distribution of wave energy as a function of wave direction θ , the first discussions of the spectral shape were done in terms of the direction-integrated spectrum $E(f)$. Phillips (1958) proposed that the non-dimensional spectrum $\alpha(f) = E(f)(2\pi)^4 f^5 / g^2$ is constant at high frequencies, because in that range all waves are breaking and thus have the same self-similar shape and the energy level “saturates”. The main focus of the present paper is how we go back from a direction-integrated view of the spectrum to a full two-dimensional spectrum.

The idea of saturation was generalized to a two-dimensional spectrum by Phillips (1985) who proposed that the degree of saturation, which is a non-dimensional quantity,

$$B(k, \theta) = k^3 E(k, \theta) \quad (3)$$

determines the geometry of the surface and the form of the source terms. Hereinafter we will use either wave frequency f or wavenumber k for the spectral dimension, exchanging one for the other using linear wave theory. In practice we note that the wavenumber spectrum is less affected by non-linear effects than the frequency spectrum and may thus be preferred (Leckler et al., 2015). Phillips introduced the idea that the dissipation should be related to the length of breaking crests $\Lambda(k, \theta)$. Phillips (1985) proposed that, for a smooth enough spectrum, is possible to use $B(k, \theta)$ as a measure of the steepness and parameterize $S_{ds}(k, \theta)$ as a function of $B(k, \theta)$. In measurements, it is much more difficult to define breaking probabilities and dissipation rates for different spectral components. Early measurements by Banner et al. (2000) focused on dominant waves, and found that there is a threshold-like behavior for breaking probabilities as a function of a dominant wave steepness. The next step was to extend this to the frequency spectrum based on observations by Banner et al. (2002). The first attempts failed to produce a reasonable energy balance and spectral shape. In particular, the measurements suggested that short waves break more often in the presence of longer waves (Babanin & Young, 2005). This observation is very important and should be the topic of much more research. At present, a full theory for the modulation of wave breaking and associated dissipation rates of short waves is still missing and many different physical processes have been proposed to explain this behavior, leading to a wide range of parameterizations.

For example, Banner et al. (1989) observed that the passage of a breaking front with a phase speed vector $\mathbf{C}(\mathbf{k}')$ may “wipe out” all slower waves with a phase speed vector $\mathbf{C}(\mathbf{k})$. This effect was parameterized by (Ardhuin et al., 2010), assuming that any breaking wave instantly dissipates a fraction $|C_{cu}|$ of the energy of all shorter waves provided that the short wave frequency is less than r_{cu} times the long wave frequency, giving a dissipation term

$$S_{ds,cu,-}(k, \theta) = C_{cu} N(k, \theta) \int_{k' < r_{cu}^2 k} |\mathbf{C}(\mathbf{k}) - \mathbf{C}(\mathbf{k}')| \Lambda(\mathbf{k}') d\mathbf{k}', \quad (4)$$

in which C_{cu} is a tuning factor of order -1, and we note that the dissipation rate is relatively higher for short waves travelling against the long breaking waves. This expression led to the first successful practical wave model based on a saturation dissipation, that strongly reduced wave model errors and was implemented in most operational wave forecasting centers starting with Météo-France and NCEP in 2012, followed by Environment Canada, the UK Met Office, and finally ECMWF as of June 2019.

However, these parameterizations are far from perfect. First of all, the typical balance of source terms led to a high frequency spectrum tail proportional to $f^{-4.5}$ and thus it still required an imposed parametric tail for the high frequencies. This parametric tail forces the spectrum to decay like f^{-5} from the spectral level at a frequency f_t set to be 2.5 times the windsea mean frequency. In practice the parameterizations based on Ardhuin et al. (2010) produce energy levels at f_t , and thus for the entire tail, that is rather high for young waves and winds over 18 m/s. A high tail level produces a very high drag coefficient via the quasi-linear effect. Still the resulting energy balance produces wave heights that match observed wave heights up to at least 15 m (Alday et al., 2021).

On a practical side, the expression in eq. (4) involves a relatively costly integral because the norm of the phase velocity difference varies with the direction of the short and the long waves. This integral was left out in the ECMWF implementation. As an alternative, a good approximation is obtained by using the difference of the norms,

$$S_{ds,cu,+}(k, \theta) = -C_{cu} N(k, \theta) \int_{k' < r_{cu}^2 k} (|\mathbf{C}(\mathbf{k})| - |\mathbf{C}(\mathbf{k}')|) \Lambda(\mathbf{k}') d\mathbf{k}', \quad (5)$$

132 with C_{cu} a tuning factor of order 1.

133 2.1 The parameterization by Romero (2019)

Romero (2019) started from recent observation of spectral shapes (Romero & Melville, 2010) breaking probabilities (Sutherland & Melville, 2015) and dissipation rates. He was the first to parameterize $\Lambda(\mathbf{k})$ as a function of the two-dimensional saturation $B(k, \theta)$ without any integration in frequency or direction,

$$\Lambda(\mathbf{k}) = \frac{l}{k} \exp\left(-\frac{B_r}{B(\mathbf{k})}\right) M_L(\mathbf{k}) M_W(\mathbf{k}), \quad (6)$$

where $l = 3.5 \times 10^{-5}$ is a dimensionless constant, $B_r = 0.005$ is a threshold for the 2-dimensional saturation spectrum, that is related to the threshold for wave breaking (Banner et al., 2000). The two multiplicative terms M_L and M_W that directly modulate the breaking probability are there to parameterize the “cumulative dissipation effect”. The idea is that short waves are modulated by long waves, making the short waves steeper on the crests of the long waves and thus more likely to break. Donelan (2001) formulated that kind of effect using a “partially integrated mean square slope”, for all waves longer than k ,

$$\text{mss}(k) = \int_0^{2\pi} \int_0^k k'^2 E(k', \theta) dk' d\theta, \quad (7)$$

which gives the same effect for all short waves and long wave directions. The first term M_L in eq. (6) is similar to Donelan’s dissipation as it uses $\text{mss}(k)$ with an added cosine-squared directional dependency that could be loosely justified by the modulation theory of Peureux et al. (2021),

$$M_L(k, \theta) = \left[1 + 400\sqrt{\text{mss}(k)} \cos^2(\theta - \theta_m)\right]^{1.5}, \quad (8)$$

134 where θ_m is the energy-weighted mean wave direction for the entire wave spectrum, hence
135 close to the direction at the peak frequency. A discussion of this particular choice is de-
136 ferred to Section 4.

The second term, M_W is a function of the wind speed and was added to help the model reproduce the transition between the f^{-4} and f^{-5} regions of the wave spectrum, or $k^{-2.5}$ to k^{-3} when considering wavenumber spectra (Long & Resio, 2007; Lenain & Melville, 2017),

$$M_W(k) = (1 + D_W \max\{1, k/k_o\}) / (1 + D_W) \quad (9)$$

with $k_o = g[3/(28u_*)]^2$ corresponding to the scale at which the spectrum was observed to transition from $k^{-2.5}$ to k^{-3} , and D_W is a dimensionless factor with recommended values of 0.9 when the DIA is used and 2 when exact nonlinear wave interactions are computed. We finally note that the dissipation source term $S_{ds}(\mathbf{k})$ is taken to be proportional to $\Lambda(\mathbf{k})$ with a dissipation rate per unit breaking crest length that is a function of a direction-integrated saturation level $B(k)$,

$$b(k) = C_{ds}^{\text{sat}} \left(\sqrt{B(k)} - \sqrt{B_T} \right)^{2.5} / g^2, \quad (10)$$

with $B_T = 0.0011$ a direction-integrated saturation threshold, giving the dissipation source term

$$S_{ds}(k, \theta) = b(k) \frac{\Lambda(k, \theta) c^5}{g^2}. \quad (11)$$

137 Romero (2019) only replaced the breaking parameterization (including the cumu-
138 lative part) of Ardhuin et al. (2010), keeping all other aspects, including the swell dis-
139 sipation based on Ardhuin et al. (2009) and wind-wave generation that was adapted from
140 Janssen (1991). The parameterization by Romero (2019) can therefore be chosen in the

WAVEWATCH III model by using the “ST4” option for S_{in} and S_{ds} parameterizations, and only changing the value of a few model parameters, as listed in Table 1. The simulations using the original for of Romero’s dissipation are given the identification number “700” in the following.

Table 1. Choices of parameterizations, methods and parameter adjustments for the different models that use the “ST4” switch in WAVEWATCH III version 7. The choice $n_B=1$ corresponds to the choice of saturation definition given by Ardhuin et al. (2010), while $n_B=3$ uses the local saturation defined by Romero (2019).

run:	default	$C_{\text{cu}} = 0.3$	700	702	704	700-WRT	702-WRT	702-GQM	707-GQM
S_{nl}	DIA	DIA	DIA	DIA	DIA	WRT	WRT	GQM	GQM
n_B	1	1	3	3	3	3	3	3	3
C_{ds}			-3.8	-3.8	-3.8	-3.8	-3.8	-3.8	-2.0
C_{cu}	-0.4	0.3	0	0.3	0.3	0	0.3	0.3	0.4
M_W			0.9	0	0.9	2.0	0.0	0.	2.0
C_t	0	0	0	1	1	0.0	1	1	1
s_u	0.3	0.2	0.3	0.2	0.0	0.3	0.0	0.0	0.0

We now illustrate the effects of source term parameterizations on simulated waves in a very simple idealized situation, representing a spatially uniform ocean starting from rest with constant 10 m/s wind. Because Romero adjusted all parameters to reproduce the growth of wave heights given by the ST4-default parameterization (Ardhuin et al., 2010), there is little difference in wave heights, as shown in Fig. 1.a. The interesting results brought by the T700 parameterization is that it can produce a shape of the spectrum tail that is close to a f^{-5} shape, for frequencies above 0.6 Hz but still a little too high (Fig. 1.b). In the case of the standard ST4 and ST6, that shape was imposed above a frequency f_t that is a constant times the mean frequency of the windsea, applying the same directional distribution $M(f, \theta)$ for all f above f_t . This imposed tail is one of the reasons why the ratio of cross-wind (mssc) to down-wind (mssd) mean square slopes is much higher with T700, as shown in Fig. 1.c. We note that these slope variances are only integrated up to 1 Hz (1.5 m wavelength), and we have added the contribution of waves with $f > 1$ Hz, using Elfouhaily et al. (1997). Because 70% of the slope variance is carried by waves shorter than 1.5 m, and the Elfouhaily et al. (1997) spectrum is poorly constrained at wavelengths from 0.2 to 3 m, a direct comparison with observed ratios mssc/mssd is a little premature and will not be pursued here. An alternative validation performed by Romero and Lubana (2022) uses measured slope variance in the presence of oil slicks (C. Cox & Munk, 1954), but is only qualitative because the effect of the slick on the shape of the wave spectrum is not exactly known.

A more dramatic difference is found for the overlap integral $I(f)$. As noted by Romero and Lubana (2022), $I(f)$ given by T700 can be more than 10 times the value given by any other parameterization, with values around 0.1 for frequencies above 3 times the wind-sea peak frequency, consistent with stereo-video data (Leckler et al., 2015; Peureux et al., 2018). An interesting property is that the second-order wave field at large wavelengths has a power spectrum density at frequency $f_s = 2f$ that is proportional to $E^2(f)I(f)$. These components generate acoustic-gravity modes (C. S. Cox & Jacobs, 1989), seismic modes (Hasselmann, 1963) and microbaroms (Brekhovskikh et al., 1973), as reviewed by Ardhuin et al. (2019) and De Carlo et al. (2020). As a result, any underwater acoustic or seismic measurements at frequency $2f$ will be proportional to $E^2(f)I(f)$ (Farrell & Munk, 2008; Duennebier et al., 2012; Peureux et al., 2018), with the proportionality coefficient varying with depth and local sediment properties (Ardhuin et al., 2013). A factor 10 difference between modeled seismic response and data can be largely due to

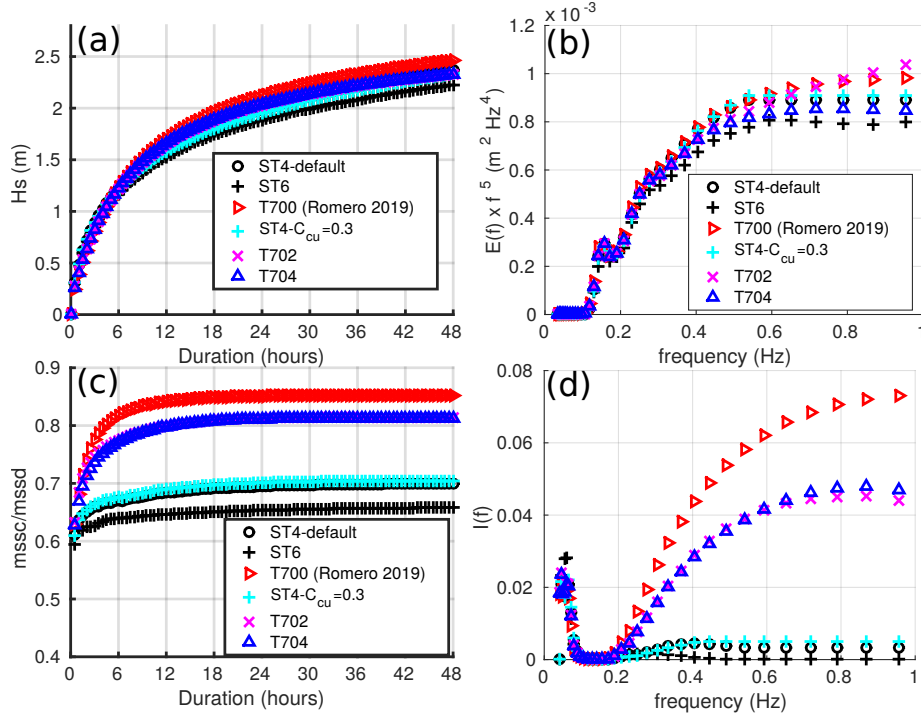


Figure 1. Evolution of (a) wave height (b) cross-wind over down-wind mean square slopes ratio, for a uniform ocean starting from rest with 10 m/s wind, and spectral distribution of (c) saturation level and (d) overlap integral after 30 hours of integration. Results with existing parameterizations based on Ardhuin et al. (2010, ST4) and Rogers et al. (2012, ST6) are shown for reference, together with Romero (2019) and several proposed adjustments (see Table 1).

uncertainties in the seismic mode generation and dissipation (Ardhuin et al., 2013), but we expect that these effects are linear and only a function of location and frequency. Therefore, the observed temporal variation of underwater acoustic data should clearly discriminate between different parameterizations, as we shall see in Section 3.

In order to further improve on the parameterizations it is interesting to expose the features that give this spectrum behavior, namely the proper levelling of the direction-integrated saturation level $f^5 E(f)$ and the directional broadening that gives these high $I(f)$ values. A distinctive feature of Romero (2019)’s parameterization is that both the dissipation term and the cumulative effect are highly directional. Thus, for directions more than 90 degrees away from the wind, if the value of $B(k, \theta)$ is not high enough there is no dissipation at all, and since the wind input is zero (or weakly negative) the only source of energy for these very oblique waves is the non-linear energy flux. As a result, whatever little flux of energy comes from S_{nl} can accumulate to a significant energy level. Figure 2 shows the inverse time scales S_{ds}/E associated to dissipation and the resulting directional spectra distribution at frequencies 0.5 Hz and 1 Hz.

The first striking feature is that the previous parameterizations have a nearly isotropic dissipation time scale E/S . The use of a partial directional integration of $B(k, \theta)$ in the ST4-default of Ardhuin et al. (2010) gives a slightly larger dissipation in the wind direction compared to 30° away from the wind, but the dissipation remains relatively high for waves against the wind. In contrast, the relative dissipation S/E from Romero (2019) goes to zero for wave directions 180 to 360° , allowing the spectrum to grow “broad shoulders” with high energy levels for directions 60-120 away from the wind, and still zero in

the direction opposite to the wind. We note that a minor change in the cumulative term using eq. (5) with $S_{cu} = 0.3$ instead of eq. (4) slightly increases the width of the ST4-default spectra (cyan '+' symbols in Fig. 1 and 2). But this effect is weak, and the dissipation rate is still high for the large oblique angles relative to the wind. We may combine this cumulative effect with the one used by Romero (2019) to get some control over the magnitude of the “broad shoulders”. Here we have proposed two versions of the parameterization. In T702 Romero’s cumulative term is simplified by removing the wind dependent part and the isotropic cumulative term of eq. (5) is added with $S_{cu} = 0.3$. This gives almost the same direction-integrated spectrum at high frequencies, as shown in Fig. 1.b, but a much lower overlap due to the finite dissipation time scales (5000 s at 0.5 Hz, 1000 s at 1 Hz). Alternatively, the T704 parameterization combines both cumulative effects, in which case the wind sheltering can be removed ($s_u = 0$) and a good high frequency tail level can be obtained, very similar to the default ST4 parameterization and the typical observed saturation level (Leckler et al., 2015).

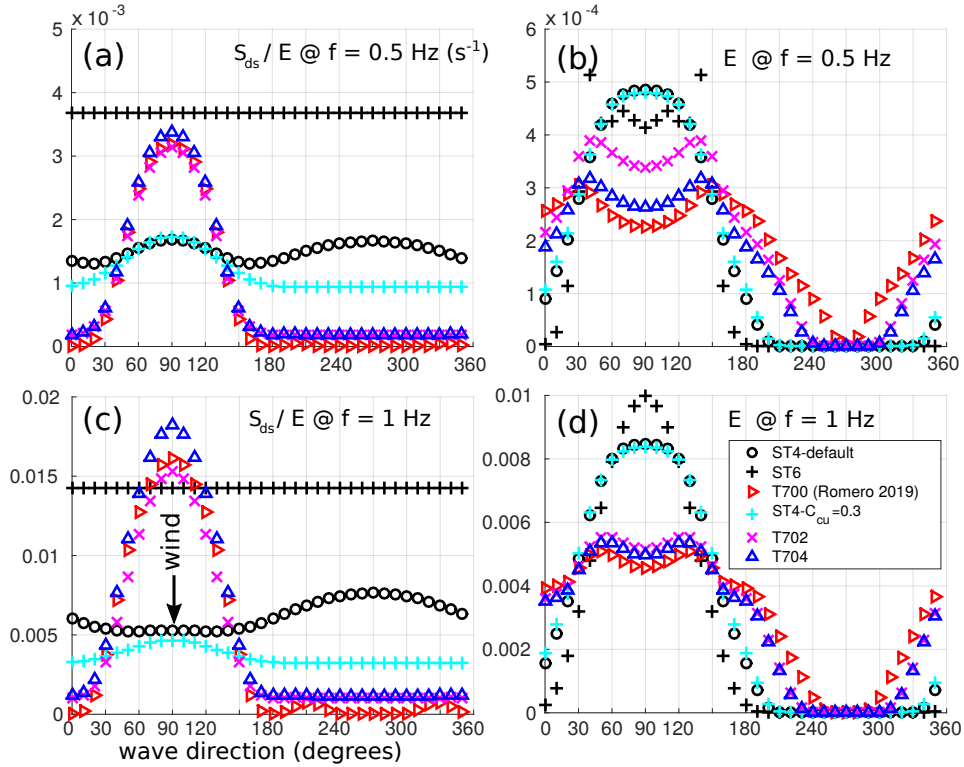


Figure 2. Inverse dissipation time scale S_{ds}/E and directional spectrum shape $E(f, \theta)$ for frequencies 0.5 Hz and 1 Hz. These are obtained after 30 hours of simulation for a uniform ocean with a constant wind speed of 10 m/s blowing in direction 90° .

Because the DIA is a poor approximation of the full non-linear interaction, it is interesting to check on the effect of using the full interaction which is computed here using these two methods approaches. Either the method of Webb (1978) and Tracy and Resio (1982) (hereinafter WRT) as implemented by van Vledder (2006), or the Gaussian Quadrature Method (GQM) of Lavrenov (2001), as implemented by Michel Benoit and optimized by Gagnaire-Renou et al. (2010). The GQM method relies on a change of variables for the resonant interactions that contribute to the source term $S_{nl}(f, \theta)$, for components (f, θ) interacting with (f_1, θ_1) , (f_2, θ_2) and (f_3, θ_3) , and transform to an integral over 3 dimensions that are f_1/f , θ_1 , and $f_2/(f+f_1)$. Results shown here for GQM

employ a coarse integration discretization using 11, 6 and 6 points along the three resonant integration dimensions, and we verified that the finer resolutions only enhanced the peaks in frequency and directional space by about 10%. Following Gagnaire-Renou (2010) we also filter out quadruplets with coupling coefficients lower than 0.05 times the maximum, and we have also added a filtering out of quadruplets at frequencies for which $f^5 E(f) < 5 \times 10^{-5} \text{ m}^2 \text{ s}^{-4}$. We note that each of these two filtering steps typically reduced the computation time by a factor 2, with no visible impact on the spectral shape. The only adjustment made to the other parameters follows the recommendation of Romero (2019) with the wind modulation coefficient D_w in eq. (9) changed from 0.9 to 2. This increased value of D_w was not sufficient to obtain a correct energy balance at high frequency, hence we also proposed a T707 adjustment that uses a reduced dissipation coefficient C_{ds} in eq. (10), similar to what is usually done when replacing the DIA method with exact interactions (Banner & Young, 1994), and we kept the wind sheltering coefficient at zero, as in the T704 adjustment with the DIA. We also note that model results with directional discretizations using 36 directions or 24 directions give very similar result, which is interesting for practical applications since the GQM, and the model in general, is faster when using 24 directions as we have chosen to use in Section 3.

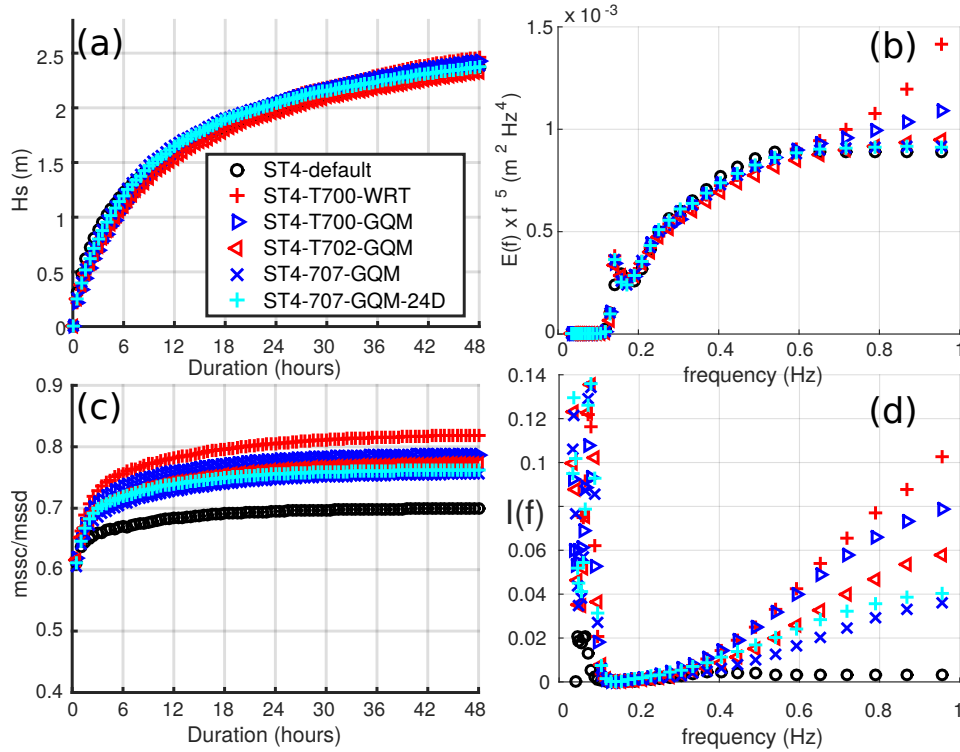


Figure 3. Same as Figure 1, for simulations using exact methods for the non-linear 4-wave interactions.

Among all the runs obtained with exact interaction methods the only one that stands out with large cross-wind slopes and overlap integrals is “ST4-T700-WRT”, the one obtained without the isotropic cumulative effect of long wave breaking wiping out the shorter waves. Whereas ST4-T700-GQM is supposed to compute the exact same thing we note that the higher frequencies differ slightly with a higher energy level and larger cross-wind energy when the WRT method is used. By changing the number of model frequencies, and changing the maximum model discrete frequency f_{\max} we have found that the WRT

method as implemented often develops a spurious tail level for $f > 0.7f_{\max}$. This effect is much less pronounced with the GQM implementation.

In order to understand the qualitative difference between DIA and exact calculations, it is useful to look at the energy balance as a function of direction, and in particular the relative dissipation rate S/E , shown in Fig. 4. Contrary to the case with the

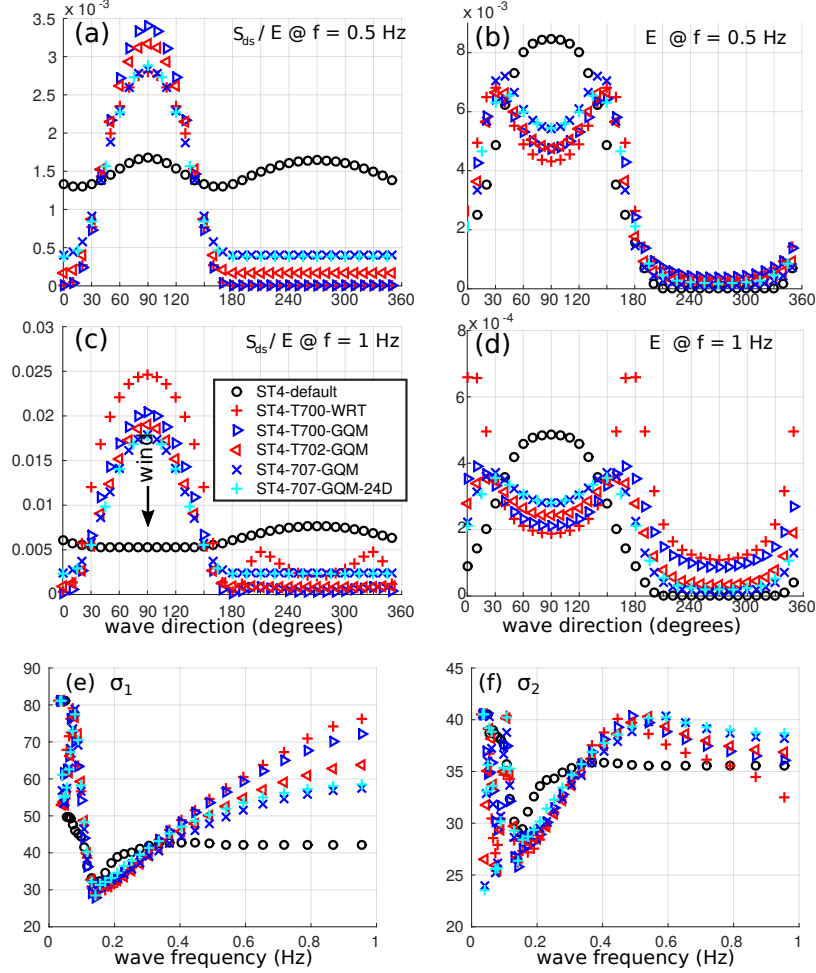


Figure 4. Same as figure 2, for simulations using exact methods for the non-linear 4-wave interactions, with the addition of directional spreads σ_1 , defined from a_1 and b_1 directional moments, and σ_2 , defined from a_2 and b_2 directional moments following Kuik et al. (1988).

DIA, the full interactions are able to fill all directions with some energy, including directions opposite to the wind, in particular at high frequencies, a phenomenon that has long been observed with High-Frequency (HF) coastal radars (Crombie et al., 1978). This effect was first modelled by Lavrenov and Ocampo-Torres (1999) in simulations without dissipation. The 17 dB difference between upwind and downwind energy levels for 0.5 Hz is compatible with the typical 20 dB difference in energy levels for wave upwind and downwind as recorded by 25 MHz HF radars (Kirincich, 2016). At 1 Hz, corresponding to $k = 4$ rad/m, the smaller difference with the T700-WRT simulation between upwind and downwind energy levels is a little surprising but no coastal radar data is available to probe these frequencies, and the stereo-video data reported by Peureux et al. (2018) in similar conditions is not conclusive due to a noise level of $E(k, \theta)$ that is probably ob-

scuring the low energy level of waves opposing the wind. Other parameters like the lobe separation and lobe ratio (ratio energy in peak direction to energy in the wind direction) are overestimated at 1 Hz by ST4-T700-WRT, and associated with the spurious tail level (the lobe ratio at 1 Hz is identical to ST4-T700-GQM when WRT is used with a maximum model frequency of 1.5 Hz, not shown). We find that the overlap integral is probably underestimated by the T707 parameterization, compared to the stereo-video data reported by Peureux et al. (2018). We also note that the high level of upwind energy at 1 Hz is large with T700-GQM and reduced by a factor 2 with 702-GQM which as a dissipation time scale of 600 s for upwind waves compared to 50 s for downwind waves. One way to keep some of the general behaviour of the source terms when also using a cumulative dissipation term given by eq. (5) is to make sure that it only acts at high enough frequencies, for example with $r_{cu} > 2.5$. Further investigation of measured spectra in steady or turning winds can probably be used for additional testing of the parameterizations.

We also note that the two directional spreads that can be measured by directional buoys have different behaviors in from narrow bimodal spectra to broad bimodal spectra as shown in Fig. 4e,f. Indeed the σ_1 spread is defined from the a_1 and b_1 directional moments, and is maximum when the same amount of energy is found in opposite directions (i.e. when both a_1 and b_1 are zero. In constrast, σ_2 -which is called σ^* by Kuik et al. (1988)- is maximum when both a_2 and b_2 are zero which happens when the same amount of energy is found in perpendicular directions. Hence σ_2 peaks at frequencies around 0.5 Hz where the two lobes are almost perpendicular and decreases as they spread further apart, so that σ_1 keeps increasing towards higher frequency when σ_2 decreases. This exact same behavior is very well described by Ewans (1998).

3 Validations at global scale

We evaluate the parameterizations described above at the global scale. Our model configuration uses a regular grid in latitude and longitude with a 0.5 degree step, extending to 80 degrees north. We used a spectral grid with 24 directions and 36 frequencies. Frequencies are exponentially spaced from 0.034 Hz to 1 Hz, with a constant ratio of 1.1 from one frequency to the next. Besides hourly winds from the fifth European Reanalysis ERA5 (Hersbach et al., 2020), the model uses daily sea ice concentration and the monthly iceberg mask from Ifremer CERSAT, and daily surface currents from Mercator-Ocean reanalysis GLORYS.

3.1 Wave heights

As demonstrated by Ardhuin et al. (2010), wave heights from global-scale wave models are most sensitive to parameters defining the the swell dissipation, and any change to the wave breaking dissipation can have an impact on the wind-sea to swell transition and thus on the energy radiated into swell. We thus repeated the parameter adjustment procedure defined by Alday et al. (2021), using the distribution of wave heights measured by Jason-2 for the year 20011, as provided in the ESA Sea State Climate Change Initiative version 1 dataset (Dodet et al., 2022). We recall that, following Leckler et al. (2013), we parameterize swell dissipation due to air-sea friction (Ardhuin et al., 2009) as a combination of viscous and turbulent terms with a transition at a Reynolds wavenumber Re_c spread out over a range of values s_7 , in order to represent a Rayleigh distribution of wave heights (Perignon et al., 2014; Stopa et al., 2016). We ran the model with either T702 and the DIA or T700 and the GQM method. Both model runs are compared to the T475 which differs from the default ST4 by a small adjustment on the swell dissipation parameters (Alday et al., 2021). Here the value of s_7 was reduced from 432000 for T475 and T700-GQM to 360000 for T702, and the swell dissipation factor was reduced from 0.66 for T475 and T700-GQM to 0.6 for T475. We also note that T475 and T702 use

a wind-wave growth parameter $\beta_{\max} = 1.7$ while T700-GQM uses $\beta_{\max} = 1.6$, which is consistent with the general reduction of other source terms when replacing the DIA with an exact method (Banner & Young, 1994). These adjustments were performed for the year 2011.

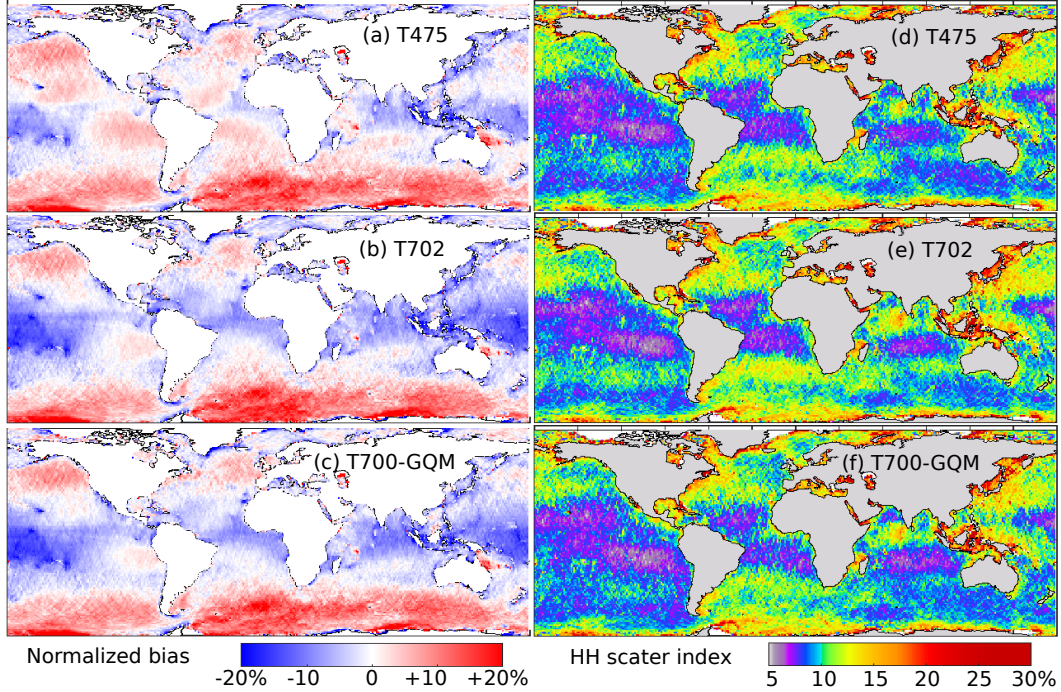


Figure 5. (a,b,c) Normalized mean difference in significant wave height between model runs and satellite altimeters for the entire year 2007 and (c,d,e) the Hanna-Heinold scatter index as defined by (Mentaschi et al., 2013).

We will now verify model results using independent data for the year 2007 that combines four different altimeters (GFO, Envisat, ERS-2 and Jason-1) provided in the ESA Sea State Climate Change Initiative version 1 dataset (Dodet et al., 2022). We also note that any adjustment is specific to the properties of the wind forcing. As mentioned above, we use winds from ERA5, which is known to have some regional biases (Belmonte Rivas & Stoffelen, 2019). To our knowledge this is the first publication discussing a global-scale 1-year long simulation using an exact calculation of 4-wave interactions. We used the “coarse” GQM integration settings proposed in (Gagnaire-Renou, 2010) and used in (Beyramzadeh & Siadatmousavi, 2022), with the same filtering described in the previous section: a first filtering on the coupling coefficient that removes half of the quadruplets (leaving around 800 quadruplets for each spectral component, compared to 2 for the DIA) and a second filtering based on the value of $E(f)f^5$, so that on average the S_{nl} term is not computed for half of the spectral components, typically for the low frequency swells. We verified at a few buoy locations in the Pacific that this second filtering had a minor impact on the low frequency energy levels, which was typically reduced by under 5% for frequencies under 0.06 Hz. The CPU time was 7.5 times longer for the full model using GQM compared to the DIA, with 45 hours of run time over 432 computational nodes. We note that a typical 6-day global forecast would typically take only one hour with the same set-up.

Wave heights in simulations with T702 and T700-GQM dissipation parameterization are very close to those obtained with T475. For wave heights, the mean difference

is within $\pm 2\%$ locally (Fig. 5b,c), with some stronger negative biases in the tropical west Pacific when using the new parameterizations. Random differences are also similar, with the Hanna-Heinold scatter index (Mentaschi et al., 2013) increasing from 6% in the trade wind areas to 15% and more along East coasts and in enclosed seas (Fig. 5d,e,f). We note that the random error of denoised 1 Hz altimeter measurements is of the order of 7% for the data used here (Dodet et al., 2022). We thus expect that in the trade wind areas most of the difference between model and satellite data is caused by random errors in satellite data. Typically the T700-GQM run gives a lower random differences than T475 in the Pacific, but larger values in the South Atlantic, and they have the exact same area-weighted averaged HH index of 10.4%, compared to 10.7% for T702.

Although these differences are small, some systematic deviations are revealed when data points are gathered for a given measured H_s , as presented in Fig. 6 for the same year 2007. Simulations with T702 and T700-GQM have a reduced bias compared to T475

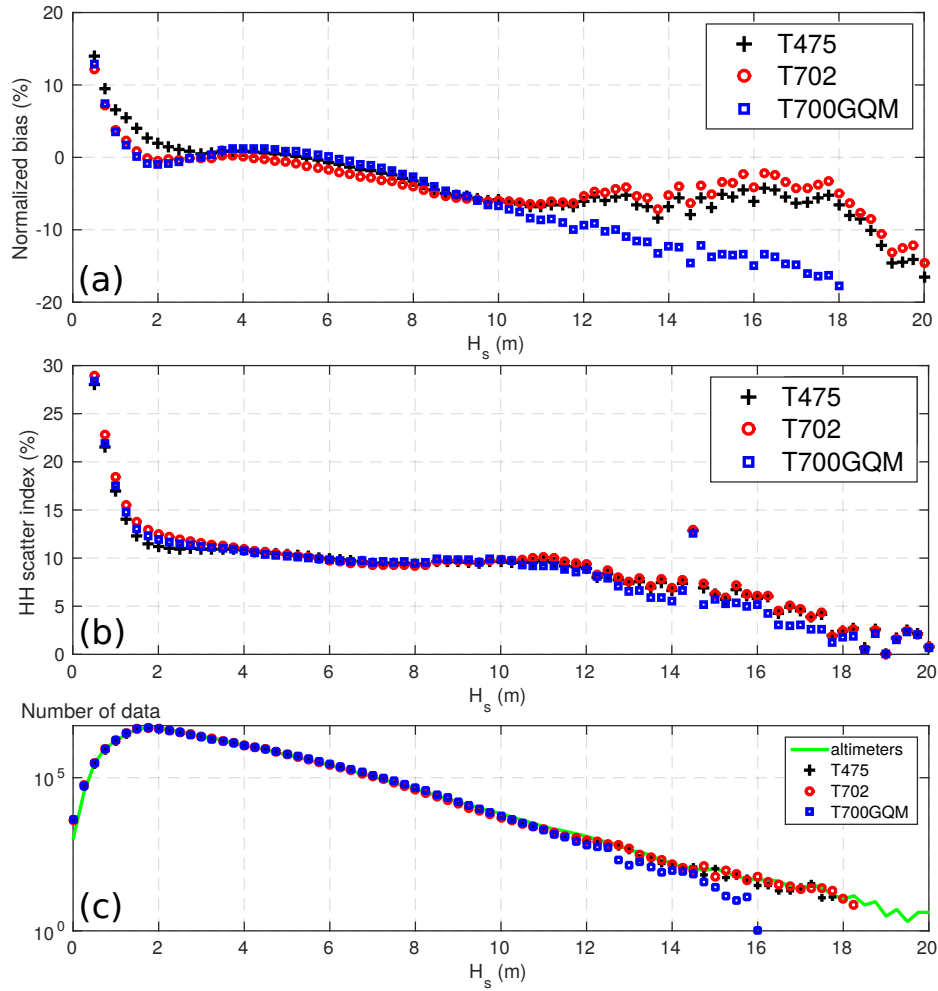


Figure 6. Model global performance with different parameterizations as a function of the wave height: T475, T702 and T700-GQM. Wave heights performance parameters for year 2011 (WW3 - Jason-2). (a) H_s NMD, (b) HH scatter index.

for wave heights in the range 0-4 m, but a higher scatter around the observed values. We suspect that most of these differences may be associated to swell dissipation. However, it is also possible that the mean direction that Romero (2019) used for the cumulative

term may be sensitive to the presence of swell which could also increase the scatter. Detailed case studies will be needed to clarify this issue.

For very large wave heights altimeters are usually most accurate, and they are consistent with other data up to 20 m wave height (Hanafin et al., 2012). Wave heights over 10 m account for 0.06% of the full altimeter record, but they are hugely important in defining extremes both locally and remotely through the radiation of swells (Hoeke et al., 2013). For that range the T700-GQM gives a much lower bias but also a lower scatter index. The analysis of this behavior is beyond the scope of the present paper, but we suspect that feedback of the spectrum tail on wind wave growth via the quasi-linear effect is important. Examination of a few cases suggest that the T475 and T702 runs give tail levels much higher than T700-GQM for the high winds found in these cases, contrary to what was shown for 10 m/s winds in the previous section. We also recall that the wind input parameterization of (Janssen, 1991) assumes a tail decreasing like f^{-5} even in the capillary wave region, and does not even correct the dispersion relation for surface tension effects.

We may thus consider the T475 and T702 runs to be somewhat “lucky” in providing probably wrong spectral level and wind-wave growth term that leads to a correct growth of H_s for $H_s > 10$ m. Efforts to resolve this are underway, and various observations of the spectral tail level and its variability (Yurovskaya et al., 2013) associated with remote sensing data (Ryabkova et al., 2019) and theoretical work (Janssen & Bidlot, 2021) may lead to more realistic spectra and wind stress. In this context, characterized by very few detailed spectral wave measurements, underwater acoustic data may provide interesting constraints on the source terms. In the following section we use data acquired in the deep ocean north of Hawaii by Duennebie et al. (2012), which covers wind speeds up to 17 m/s.

3.2 Underwater acoustic data and directional spectral tail properties

Recent model developments show that one could predict the variability of the seismic or acoustic wave energy at acoustic frequencies f_s in the range 0.08 to 0.4 Hz using a wave model like WAVEWATCH III. However, underwater acoustic data show that wave-induced signal extend all the way to 60 Hz (Farrell & Munk, 2010; Duennebie et al., 2012). Ardhuin et al. (2013) suspected that the poor acoustic model performance for $f_s > 0.4$ Hz was caused by an unrealistic directional wave spectra shape. This question was also discussed by Peureux and Ardhuin (2016) who proposed parameterizations of the directional distribution that could explain the observed acoustic levels.

One general difficulty of using seismic or acoustic data generated by the double-frequency mechanism of Longuet-Higgins (1950) and Hasselmann (1963) is that the absolute magnitude of the signal is influenced by bottom properties, as already noted by Abramovici (1968). Also, at the lower frequencies typically $f_s < 0.3$ Hz, the signal can propagate over thousands of kilometers along the wave guide that is constituted by the water layer and the upper crust and sediment layers. As a result, it is not straightforward to link the local wave properties and the local acoustic field. However, for the higher frequencies, as the scale over which the signal is attenuated becomes shorter than the scale at which we can consider the sea state to be homogeneous, there should be a linear relation between the local value of $E^2(f)I(f)$ and the local seismic or acoustic power.

Farrell and Munk (2010) have analyzed ocean bottom hydrophone data in 5000 m depth and showed that the acoustic level for frequencies 1 to 6 Hz transitions from a saturated level when the wind is above 5-6 m/s to a “bust” very low level when the wind drops below this value. This is expected to be caused by a narrowing of the spectrum as the wind sea peak frequency goes down closer to 0.2 - 0.5 Hz, and thus a very strong reduction of the overlap integral $I(f_s)$, by a factor at least 10. Because most parameterizations - including T475 - use a diagnostic tail that made $M(f, \theta)$ constant above some

frequency f_t , the value of $I(f)$ is frequency-independent above f_t and has a narrow range of variation. Romero and Lubana (2022) showed that T700 gave a much higher value of the overlap integral but did not directly compare predicted acoustic or seismic data to measurements.

Here we use data from the ALOHA cabled observatory provided by Duennebie et al. (2012), and compare the relative variation of local predicted seismo-acoustic source proportional to $E^2(f)I(f)$ with the ocean bottom acoustic power. The employed data corresponds to acoustic power spectra from 26 February to 31 December 2007, taking the median over 3 hours and compare it to the time-centered model snapshot computed from the local wave spectrum.

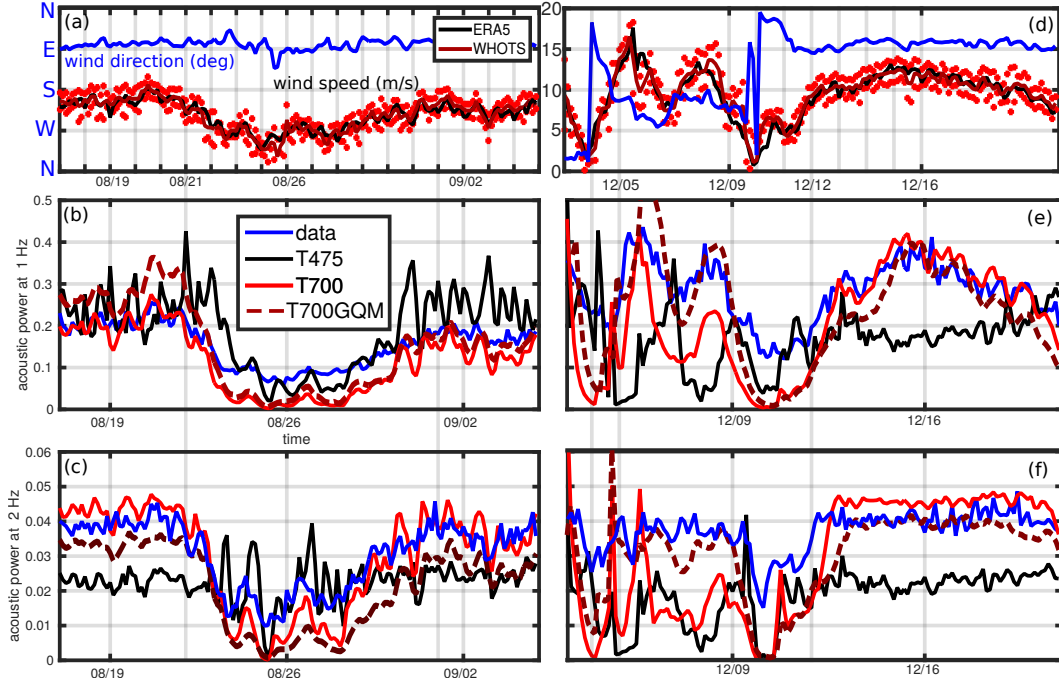


Figure 7. Timeseries of 3-hourly wind speed and direction and 10-minute averaged measurements (panels a,d) and noise level over a few weeks of summer (a,b,c) and winter (d,e,f) in 2007 at the ALOHA Cabled Observatory, north of Ohahu Hawaii, using data provided by (Duennebie et al., 2012) and model runs T475, T700 and T700-GQM. In order to give results comparable to T700, results for T475 are multiplied by 10 for 1 Hz and 15 for 20 Hz.

Figure 7 shows time series of modeled seismic source time series and observed acoustic power for two typical time intervals with moderate (Easterly) trade winds in the summer, and a winter Southerly storm followed by intense trade winds. Note that the modeled acoustic noise was re-scaled because of the poorly known bottom amplification effect, with a larger re-scaling coefficient for T475. Farrell and Munk (2010) showed that the 2 Hz acoustic signal has a fairly constant level, here around $0.04 \text{ Pa}^2/\text{Hz}$ (Fig. 7c,f), with some occasional drops, which they called “busts”. Such busts occur in our record when the wind speed decreases below 8 m/s, from 21 August to 1st of September and from 9 December to 12 December. This behaviour is associated with 1 Hz surface gravity waves and is generally well reproduced by T700 but not by T475, which has too narrow a range of variation of the seismo-acoustic source. The rise in modeled acoustic level is delayed with T700-GQM with a saturation that is only reached when the wind speed rises to 10 m/s and the general sensitivity of the modeled acoustic level is larger with

T700 and T700-GQM, with an amplification by a factor 40 from a wind speed increase of 2 m/s to 10 m/s. While it is possible that background noise may obscure low noise levels, the analysis of Duennebier et al. (2012) suggests only a factor 10 increase for such a wind speed increase, while Farrell and Munk (2013) give a factor up to 30 (15 dB).

The behaviour at 1 Hz is more complex, and there is no simple saturation of the acoustic energy in that case, but rather a general increase of acoustic power with increasing wind speed, which in this case is exaggerated by T700 and not well followed by T475 when the wind speed exceeds 10 m/s.

Correlations between model output and measured (3-hour median) acoustic levels over the full time series are shown in Fig. 8 as a function of frequency. Clearly T475

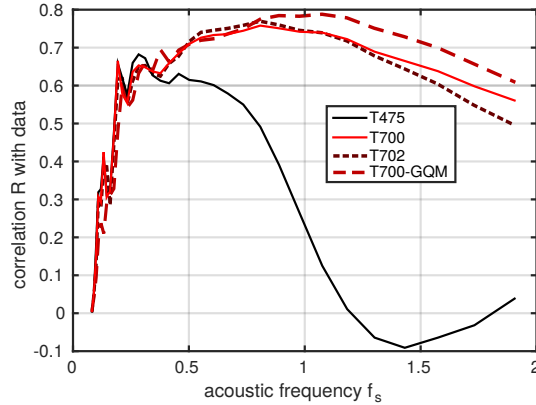


Figure 8. Correlation of modeled acoustic noise at the ALOHA observatory, north of Oahu Hawaii, for the year 2007 using data provided by (Duennebier et al., 2012) and model runs T475, T700, T702 and T700-GQM.

had very little skill for for acoustic frequencies above 0.6 Hz (wave frequencies above 0.3 Hz), and parameterizations by Tolman and Chalikov (1996) and Bidlot et al. (2005) were previously shown to be even worse (Ardhuin et al., 2013). T700 is a clear improvement, even more so when the exact non-linear calculation with GQM replaces the DIA parameterization. It would be interesting to explore higher frequencies, but this is beyond the scope of the present paper. We note that for wave frequencies in the range 0.3 to 1 Hz, the good correlation between modeled and measured acoustic noise levels (with frequencies 0.6 to 2 Hz) supports the idea that noise is mostly driven by waves propagating at angles 80 degrees or more relative to the wind direction, which requires a much larger dissipation time scale for these directions compared to the time scale in the mean wave direction.

3.3 Wave spectra

The influence of the model parameterization on directional wave spectra may be more easily interpreted with the more familiar kind of data obtained from buoys. Although buoy data may not be reliable at frequencies above 0.4 Hz, they provide separate measurements of the energy level and some measure of the directional spreading. We have chosen the CDIP station 166 located next to Station Papa in the North-East Pacific, also known by its WMO code number 46246. This instrument is a Datawel Waverider buoy maintained by Thomson et al. (2013) which generally provides accurate directional properties (O'Reilly et al., 1996).

Here we illustrate the variation of these quantities for one wave event in 2011, with low winds veering from North-westerly to an Easterly directions in the early hours of 27

January, and increasing to 13 m/s (these are uncorrected winds measured at 5 m height) with a steady Easterly direction, as shown in Fig. 9.a. The resulting sea state is thus

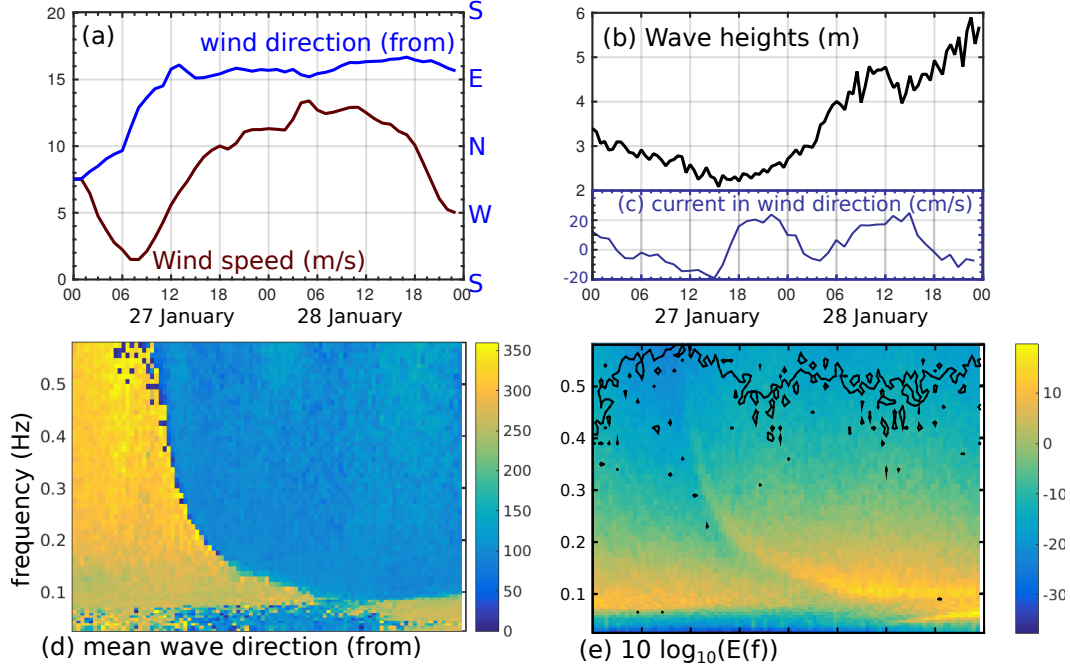


Figure 9. (a) Wind speed, wind direction and (c) significant wave height over a wind event recorded at Ocean Station Papa and nearby buoy 46246 (CDIP station 166) 27-28 January 2011. (c) Current at 15 m depth projected on the wind direction (d) shows the evolution of the mean wave direction and (e) the evolution of the wave spectrum $E(f)$, with overlaid in black the contour for the check ratio equal to 0.8.

relatively complex on 27 January with the northwesterly waves accounting for most of the wave energy and the easterly windsea progressively growing from high frequencies down to 0.15 Hz. The sea state is a more simple windsea dominated condition on January 28. Model results for different source term settings are shown in figure 10. We chose to focus on 3 spectral quantities, that are the saturation level of the spectrum, proportional to $f^5 E(f)$, the first directional spread $\sigma_1(f)$ and the second directional spread $\sigma_2(f)$ as defined by Kuik et al. (1988) and already discussed in Section 2 and Ewans (1998).

Starting from the saturation levels comes from the idea that we might possibly examine data beyond the equilibrium range in which the energy levels decrease like f^{-4} . As the transition from f^{-4} to f^{-5} is expected to occur at a frequency of the order of $f_n = 0.0225g/u_*$ (Lenain & Melville, 2017), this would be around 2 Hz for a 3 m/s wind and around 0.4 Hz for 14 m/s. In the present event this could be visible in the buoy record on 28 January. Surprisingly the spectral tail shoots up at high frequencies (black lines with dots in Fig. 10, panels in top row). The highest values of the measured tail level happen to coincide with times when the current follows the wind with speeds around 20 cm/s, and when the ratio of horizontal to vertical motion (also known as the “check ratio”) drops around 0.8 for frequencies above 0.4 Hz. We thus assume that the buoy is somewhat hampered by its mooring and may not be reliable for frequencies above 0.4 Hz. It is nevertheless interesting to examine the behaviour of the different model runs. First of all, the energy level in T475 runs are dictated by the imposed f^{-5} tail, which here limit the value

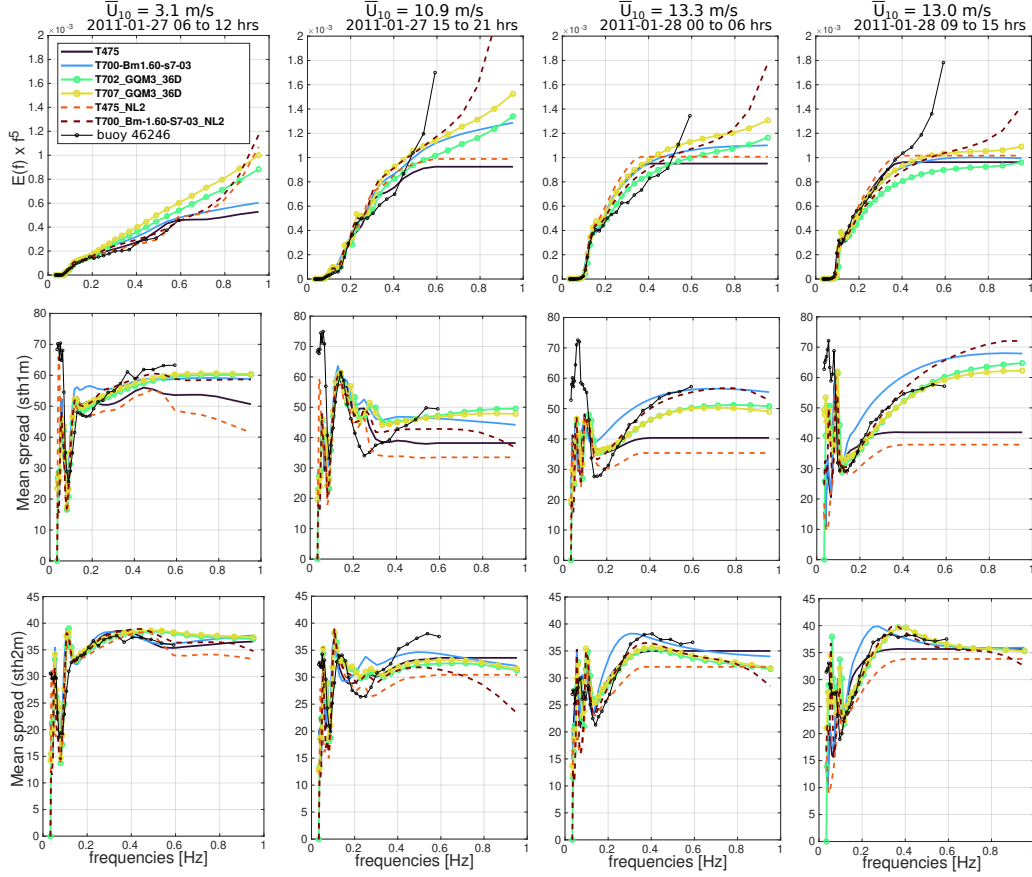


Figure 10. Modeled and measured spectrum, multiplied by f^5 (top panels), first mean spread $\sigma_1(f)$ (middle panels), and second mean spread $\sigma_2(f)$ (bottom panels).

of $f^5 E(f)$ to about $0.001 \text{ m}^2 \text{ Hz}^4$, i.e. a saturation level of $0.0005 (2\pi)^4 / g^2 = 0.008$, which is rather high. Computations without the imposed tail and using the WRT method for the exact non-linear interactions also produce sharply increasing saturation levels. This anomalous tail level is reduced when using GQM, and the tail can be adjusted to any level when a cumulative breaking term is added in T702 and T707 simulations, based on eq. (5).

Now looking at directional spread σ_1 (middle row in Fig. 10) and σ_2 (bottom row), we find that T700 has a tendency to overestimate the directional spread while T700-WRT (here T700-Bm-1.60-S7-03-NL2) has a general very good reproduction of the variations of both σ_1 and σ_2 . We note that on 28 January all parameterizations based on Romero (2019) are able to reproduce the monotonic rise in σ_1 towards higher frequencies and a maximum of σ_2 at intermediate frequencies that are typical of an increasing angular lobe separation towards higher frequencies. The T700 calculation in blue has the σ_2 peak at lower frequencies than the buoy data due to the much broader lobes produced by the DIA compared to exact non-linear calculations. We also find that T702 and T707 directional spreads are lower than measured by the buoy, suggesting that our added cumulative term is too strong and that the energy level against the wind direction may be more realistic with the original T700.

4 Discussion and conclusions

In the previous section, we have looked at the influence of different adjustments of the wave dissipation parameterization T700 by Romero (2019) and compared it to the parameterization T475 by Ardhuin et al. (2010) as modified by Leckler et al. (2013) and adjusted by Alday et al. (2021). The most profound difference introduced by Romero (2019) is a practically “directionally decoupled dissipation”: the Λ ’s are decoupled but the dissipation rates are not. This idea of decoupling was already used to justify the variation in wave energy with wind direction for slanting fetches (Donelan et al., 1985; Pettersson et al., 2010). This parameterization is the first that can give a zero dissipation rate for waves travelling at 90° from the wind and a strong dissipation rate for waves in the wind direction. This feature is capable of producing directional bimodal spectra, first reported by (Young et al., 1995), with realistic shapes, which was an important objective of Romero (2019). As expected by Romero and Lubana (2022), we have demonstrated that one particular benefit is the capability to reproduce the variability in microseism sources at high frequencies, without compromising the accuracy of wave heights. We have found that most accurate results are obtained with exact non-linear calculations that are now affordable thanks to the Gaussian Quadrature Method (GQM) proposed by Lavrenov (2001), and which we have used extensively. These calculations support the conclusion that the energy level in cross-wind and up-wind directions that is found at frequencies higher than 3 times the wind sea peak, is the result of a balance between the 4-wave interactions and a relatively very weak dissipation, compared to the dissipation in the main wave direction, thereby providing a constraint on this relative strength of the dissipation in different directions. There are still open issues with significant wave heights higher than 10 m and these will require a detailed look at wind-wave growth parameterizations and drag coefficients.

The present work was limited by the availability of large datasets with detailed directional wave measurements and reliable measurements of the short wave energy level. In particular we have made no attempt to tune the spectral level to an elusive reference and only used stereo-photo and stereo-video measurements as a weak guideline for average wind conditions (Banner et al., 1989; Leckler et al., 2013; Peureux et al., 2018). The tail level may vary widely depending on the choice of cumulative terms. However, if the cumulative term include a large near-isotropic contribution as given by eqs. (4) or (5) it will reduce the directional spread to a level that is lower than observed. We expect that video data in a wider range of conditions (including non-bimodal cases), and also drifting buoy data that may be able to accurately resolve shorter waves, will be key in the detail examination of source term behavior in a wider range of conditions, including turning winds. These data will be very useful for further validation of the direction-integrated energy level at different frequencies.

Looking back at the parameterization by Romero (2019), some ad hoc choices, not based on first principles, will probably require further testing and may open the way to future improvements. In particular the choices in the cumulative term of a cosine squared factor and a reference direction in the energy-weighted mean direction may lead to spurious directional spectral shapes in the presence of swell and in turning wind conditions as the mean direction can be anything relative to the wind. In particular, the sharp peak in modeled acoustic power on 4 December 2007 (Fig. 7) is not observed, and corresponds to a rapid turning wind in which the wind direction is around 220° and the mean wave direction (energy-weighted) is around 330° . Possibly using a mean direction weighted by orbital-velocity would perform better. That case is also associated to a very young wind sea. Another question is whether it is really necessary to have a wind parameter in the dissipation term with M_W . As we have shown, some other cumulative parameterization may perform just as well with M_W set to zero, as in our T702 variant. Although wind may directly impact wave breaking at high wind speeds (Soloviev et al., 2014) or in shoal-

ing waves (Feddersen & Veron, 2005) there is no generally established mechanism for such an effect.

Clearly much more work is needed on understanding the possible physical processes that may justify the detailed choices of Romero (2019) or any future evolution on it, and in particular much more research is needed to understand the “cumulative effect”. Without this understanding, we are left to grope in the dark. Some sensitivity analysis using indirect constraints on the spectral shape, e.g., provided by underwater acoustic data, HF radars (Tyler et al., 1974; Kirincich, 2016), and radar backscatter in general (Kudryavtsev et al., 2003; Ryabkova et al., 2019), may still be used to refine what can be realistic features in a source term parameterization. One will probably have to distinguish homogeneous conditions from more complex situations, including current gradients (Phillips, 1984; Romero, 2019).

Acknowledgments

We thank CNES for supporting this work as part of the preparation effort for several Earth Observation satellite missions including SWOT, SKIM and ODYSEA. We are forever indebted to the late Fred Duennebieer for providing ocean bottom pressure spectra. The GQM code was kindly provided by Michel Benoit in the TOMAWAC model and first adapted to WAVEWATCH III by Mostafa Beyramzadeh. Other datasets used in the present paper include in situ data from the PAPA Ocean Station provided by the OCS Project Office of NOAA/PMEL, wind time series from WHOTS, WHOI-Hawaii Ocean Time-series Site (WHOTS) mooring, which is supported in part by the National Oceanic and Atmospheric Administration (NOAA) Global Ocean Monitoring and Observing (GOMO) Program through the Cooperative Institute for the North Atlantic Region (CINAR) under Cooperative Agreement NA14OAR4320158. NOAA CPO FundRef number 100007298 to the Woods Hole Oceanographic Institution, and by National Science Foundation grants OCE-0327513, OCE-0752606, OCE-0926766, OCE-1260164 and OCE-1756517 to the University of Hawaii for the Hawaii Ocean Time-series.

Data Availability Statement

In agreement with Fred Duennebieer’s family and colleagues the bottom pressure spectral data is available at <https://doi.org/10.17882/9210>. The CDIP wave buoy data are available at cdip.ucsd.edu, ERA5 reanalysis available from <https://cds.climate.copernicus.eu> and altimeter data from the CNES/NASA/Eumetsat/NOAA mission Jason-2, reprocessed by ESA and available at dx.doi.org/10.5285/8cb46a5efaa74032bf1833438f499cc3. The WAVEWATCH III model can be downloaded from <https://github.com/NOAA-EMC/WW3>.

References

- Abramovici, F. (1968). Diagnostic diagrams and transfer functions for oceanic waveguides. *Bull. Seism. Soc. Am.*, *58*(1), 426–456.
- Alday, M., Accensi, M., Ardhuin, F., & Dodet, G. (2021). A global wave parameter database for geophysical applications. part 3: Improved forcing and spectral resolution. *Ocean Modelling*, *166*, 101848. doi: 10.1016/j.ocemod.2021.101848
- Ardhuin, F., Chapron, B., & Collard, F. (2009). Observation of swell dissipation across oceans. *Geophys. Res. Lett.*, *36*, L06607. doi: 10.1029/2008GL037030
- Ardhuin, F., Gualtieri, L., & Stutzmann, E. (2019). Physics of ambient noise generation by ocean waves. In N. Nakata, L. Gualtieri, & A. Fichtner (Eds.), *Ambient seismic noise* (pp. 69–107). Cambridge University Press.
- Ardhuin, F., & Jenkins, A. D. (2006). On the interaction of surface waves and upper ocean turbulence. *J. Phys. Oceanogr.*, *36*(3), 551–557. doi: 10.1175/JPO2862

- Ardhuin, F., Lavanant, T., Obrebski, M., Marié, L., Royer, J.-Y., d'Eu, J.-F., ...
 Aucan, J. (2013). A numerical model for ocean ultra low frequency noise:
 wave-generated acoustic-gravity and Rayleigh modes. *J. Acoust. Soc. Amer.*,
134(4), 3242–3259.
- Ardhuin, F., Rogers, E., Babanin, A., Filipot, J.-F., Magne, R., Roland, A., ... Col-
 lard, F. (2010). Semi-empirical dissipation source functions for wind-wave
 models: part I, definition, calibration and validation. *J. Phys. Oceanogr.*,
40(9), 1917–1941. doi: 10.1175/2010JPO4324.1
- Babanin, A. V., & Young, I. R. (2005). Two-phase behaviour of the spectral dissi-
 pation of wind waves. In *Proceedings of the 5th international symposium ocean
 wave measurement and analysis, madrid, june 2005*. (paper number 51)
- Banner, M. L., Babanin, A. V., & Young, I. R. (2000). Breaking probability for
 dominant waves on the sea surface. *J. Phys. Oceanogr.*, *30*, 3145–3160. Re-
 trieved from [http://ams.allenpress.com/archive/1520-0485/30/12/
 pdf/i1520-0485-30-12-3145.pdf](http://ams.allenpress.com/archive/1520-0485/30/12/pdf/i1520-0485-30-12-3145.pdf) doi: 10.1175/1520-0485(2000)030<3145:
 BPDFWO>2.0.CO;2
- Banner, M. L., Gemmrich, J. R., & Farmer, D. M. (2002). Multiscale measurement
 of ocean wave breaking probability. *J. Phys. Oceanogr.*, *32*, 3364–3374. Re-
 trieved from [http://ams.allenpress.com/archive/1520-0485/32/12/pdf/
 i1520-0485-32-12-3364.pdf](http://ams.allenpress.com/archive/1520-0485/32/12/pdf/i1520-0485-32-12-3364.pdf)
- Banner, M. L., Jones, I. S. F., & Trinder, J. C. (1989). Wavenumber spectra of short
 gravity waves. *J. Fluid Mech.*, *198*, 321–344.
- Banner, M. L., & Young, I. R. (1994). Modeling spectral dissipation in the evolu-
 tion of wind waves. part I: assessment of existing model performance. *J. Phys.
 Oceanogr.*, *24*(7), 1550–1570. Retrieved from [http://ams.allenpress.com/
 archive/1520-0485/24/7/pdf/i1520-0485-24-7-1550.pdf](http://ams.allenpress.com/archive/1520-0485/24/7/pdf/i1520-0485-24-7-1550.pdf)
- Belmonte Rivas, M., & Stoffelen, A. (2019). Characterizing ERA-Interim and ERA5
 surface wind biases using ASCAT. *Ocean Sci.*, *15*, 831–852. doi: 10.5194/os-15
 -831-2019
- Beyramzadeh, M., & Siadatmousavi, S. M. (2022). Skill assessment of different
 quadruplet wave-wave interaction formulations in the wavewatch-iii model
 with application to the gulf of mexico. *Appl. Ocean Res.*, *127*, 103316. doi:
 /10.1016/j.apor.2022.103316
- Bidlot, J., Janssen, P. A. E. M., & Abdalla, S. (2005). *A revised formula-
 tion for ocean wave dissipation in CY25R1* (Tech. Rep. No. Memorandum
 R60.9/JB/0516). Research Department, ECMWF, Reading, U. K.
- Brekhovskikh, L. M., Goncharov, V. V., Kurtepov, V. M., & Naugolnykh, K. A.
 (1973). The radiation of infrasound into the atmosphere by surface waves in
 the ocean. *Izv. Atmos. Ocean. Phys.*, *9*, 899–907 (In the English translation,
 511–515.).
- Cox, C., & Munk, W. (1954). Measurement of the roughness of the sea surface from
 photographs of the sun's glitter. *J. Opt. Soc. Am.*, *44*(11), 838–850. doi: 10
 .1364/josa.44.000838
- Cox, C. S., & Jacobs, D. C. (1989). Cartesian diver observations of double frequency
 pressure fluctuations in the upper levels of the ocean. *Geophys. Res. Lett.*,
16(8), 807–810.
- Crombie, D. D., Hasselmann, K., & Sell, W. (1978). High-frequency radar observa-
 tions of sea waves travelling in opposition to the wind. *Boundary-Layer Meteo-
 rol.*, *13*, 45–54.
- De Carlo, M., Ardhuin, F., & Pichon, A. L. (2020). Atmospheric infrasound ra-
 diation from ocean waves in finite depth: a unified generation theory and
 application to radiation patterns. *Geophys. J. Int.*, *221*, 569–585. doi:
 10.1093/gji/ggaa015
- Dodet, G., Abdalla, S., Alday, M., Accensi, M., Bidlot, J., & Ardhuin, F. (2022).
 Error characterization of significant wave heights in multidecadal satel-

- lite altimeter product, model hindcast, and in situ measurements using the triple collocation technique. *J. Atmos. Ocean Technol.*, 39, 887–901. doi: 10.1175/JTECH-D-21-0179.1
- Donelan, M. A. (2001). A nonlinear dissipation function due to wave breaking. In *Proceedings of ecwuf workshop on ocean wave forecasting, 2–4 july* (pp. 87–94).
- Donelan, M. A., Hamilton, J., & Hui, W. H. (1985). Directional spectra of wind-generated waves. *Phil. Trans. Roy. Soc. London A*, 315, 509–562.
- Duennebie, F. K., Lukas, R., Nosal, E.-M., Aucan, J., & Weller, R. A. (2012). Wind, waves, and acoustic background levels at station ALOHA. *J. Geophys. Res.*, 117, C03017. doi: 10.1029/2011JC007267
- Dulov, V. A., & Kosnik, M. V. (2009). Effects of three-wave interactions in the gravity-capillary range of wind waves. *Izv. Atmos. Ocean. Phys.*, 45(3), 380–391.
- Elfouhaily, T., Chapron, B., Katsaros, K., & Vandemark, D. (1997). A unified directional spectrum for long and short wind-driven waves. *J. Geophys. Res.*, 102(C7), 15781–15796. doi: 10.1029/97jc00467
- Ewans, K. C. (1998). Observations of the directional spectrum of fetch-limited waves. *J. Phys. Oceanogr.*, 28, 495–512. Retrieved from <http://ams.allenpress.com/archive/1520-0485/28/3/pdf/i1520-0485-28-4-495.pdf>
- Farrell, W. E., & Munk, W. (2008). What do deep sea pressure fluctuations tell about short surface waves? *Geophys. Res. Lett.*, 35(7), L19605. doi: 10.1029/2008GL035008
- Farrell, W. E., & Munk, W. (2010). Booms and busts in the deep. *J. Phys. Oceanogr.*, 40(9), 2159–2169.
- Farrell, W. E., & Munk, W. (2013). Surface gravity waves and their acoustic signatures, 1–30 hz, on the mid-Pacific sea floor. *J. Acoust. Soc. Amer.*, 134(4), 3161–3173.
- Feddersen, F., & Veron, F. (2005). Wind effects on shoaling wave shape. *J. Phys. Oceanogr.*, 35, 1223–1228.
- Gagnaire-Renou, E. (2010). *Amelioration de la modelisation spectrale des etats de mer par un calcul quasi-exact des interactions non-lineaires vague-vague* (Unpublished doctoral dissertation). Université du Sud Toulon Var.
- Gagnaire-Renou, E., Benoit, M., & Forget, P. (2010). Ocean wave spectrum properties as derived from quasi-exact computations of nonlinear wave-wave interactions. *J. Geophys. Res.*, 115, C12058. doi: 10.1029/2009JC005665
- Hanafin, J., Quilfen, Y., Ardhuin, F., Sienkiewicz, J., Queffelec, P., Obrebski, M., ... Stutzmann, E. (2012). Phenomenal sea states and swell radiation: a comprehensive analysis of the 12–16 February 2011 North Atlantic storms. *Bull. Amer. Meteorol. Soc.*, 93, 1825–1832. doi: 10.1175/BAMS-D-11-00128.1
- Hasselmann, K. (1962). On the non-linear energy transfer in a gravity wave spectrum, part 1: general theory. *J. Fluid Mech.*, 12, 481–501.
- Hasselmann, K. (1963). A statistical analysis of the generation of microseisms. *Rev. of Geophys.*, 1(2), 177–210.
- Hasselmann, K., Raney, R. K., Plant, W. J., Alpers, W., Shuchman, R. A., Lyzenga, D. R., ... Tucker, M. J. (1985). Theory of Synthetic Aperture Radar ocean imaging: a MARSEN view. *J. Geophys. Res.*, 90(C3), 4659–4686.
- Hersbach, H., Bell, B., Berrisford, P., Hirahara, S., Horányi, A., Muñoz-Sabater, J., ... Thépaut, J. (2020). The ERA5 global reanalysis. *Quart. Journ. Roy. Meteorol. Soc.*, 146, 1999–2049. doi: 10.1002/qj.3803
- Hoeke, R. K., McInnes, K. L., Kruger, J. C., McNaught, R. J., Hunter, J. R., & Smithers, S. G. (2013). Widespread inundation of Pacific islands triggered by distant-source wind-waves. *Global and Planetary Change*, 108, 128–138. doi: 10.1016/j.gloplacha.2013.06.006

- Janssen, P. A. E. M. (1991). Quasi-linear theory of wind wave generation applied to wave forecasting. *J. Phys. Oceanogr.*, *21*, 1631–1642. Retrieved from <http://journals.ametsoc.org/doi/pdf/10.1175/1520-0485%281991%29021%3C1631%3AQLTOWW%3E2.0.CO%3B2> (See comments by D. Chalikov, *J. Phys. Oceanogr.* 1993, vol. 23 pp. 1597–1600)
- Janssen, P. A. E. M., & Bidlot, J. (2021). *On the technical consequences of nonlinearity and gravity-capillary on wind-wave interaction* (Tech. Rep. No. Technical Memo 882). Research Department, ECMWF, Reading, U. K.
- Kirincich, A. (2016). Remote sensing of the surface wind field over the coastal ocean via direct calibration of HF radar backscatter power. *J. Atmos. Ocean Technol.*, *33*(7), 1377–1392. doi: 10.1175/JTECH-D-15-0242.1
- Komen, G. J., Cavaleri, L., Donelan, M., Hasselmann, K., Hasselmann, S., & Janssen, P. A. E. M. (1994). *Dynamics and modelling of ocean waves*. Cambridge: Cambridge University Press.
- Kudryavtsev, V., Hauser, D., Caudal, G., & Chapron, B. (2003). A semiempirical model of the normalized radar cross-section of the sea surface 2. radar modulation transfer function. *J. Geophys. Res.*, *108*(C3), 8055. doi: 10.1029/2001JCOO1004
- Kuik, A. J., van Vledder, G. P., & Holthuijsen, L. H. (1988). A method for the routine analysis of pitch-and-roll buoy wave data. *J. Phys. Oceanogr.*, *18*, 1020–1034. Retrieved from <http://journals.ametsoc.org/doi/pdf/10.1175/1520-0485%281987%29017%3C0845%3ATROWDT%3E2.0.CO%3B2>
- Lavrenov, I. V. (2001). Effect of wind wave parameter fluctuation on the nonlinear spectrum evolution. *J. Phys. Oceanogr.*, *31*, 861–873. Retrieved from <http://ams.allenpress.com/archive/1520-0485/31/4/pdf/i1520-0485-31-4-861>
- Lavrenov, I. V., & Ocampo-Torres, F. J. (1999). Angular distribution effect on weakly nonlinear energy transfer in the spectrum of wind waves. *Izv. Atmos. Ocean. Phys.*, *35*, 278–290.
- Leckler, F., Ardhuin, F., Filipot, J.-F., & Mironov, A. (2013). Dissipation source terms and whitecap statistics. *Ocean Modelling*, *70*(9), 62–74.
- Leckler, F., Ardhuin, F., Peureux, C., Benetazzo, A., Bergamasco, F., & Dulov, V. (2015). Analysis and interpretation of frequency-wavenumber spectra of young wind waves. *J. Phys. Oceanogr.*, *45*, 2484–2496. doi: 10.1175/JPO-D-14-0237.1
- Lenain, L., & Melville, W. K. (2017). Measurements of the directional spectrum across the equilibrium saturation ranges of wind-generated surface waves. *J. Phys. Oceanogr.*, *47*, 2123–2138. doi: 10.1175/jpo-d-17-0017.1
- Long, C. E., & Resio, D. T. (2007). Wind wave spectral observations in Currituck Sound, North Carolina. *J. Geophys. Res.*, *112*, C05001. doi: 10.1029/2006JC003835
- Longuet-Higgins, M. S. (1950). A theory of the origin of microseisms. *Phil. Trans. Roy. Soc. London A*, *243*, 1–35.
- Mentaschi, L., Besio, G., Cassola, F., & Mazzino, A. (2013). Problems in RMSE-based wave model validations. *Ocean Modelling*, *72*, 53–58. doi: 10.1016/j.ocemod.2013.08.003
- Miles, J. W. (1957). On the generation of surface waves by shear flows. *J. Fluid Mech.*, *3*, 185–204.
- O'Reilly, W. C., Herbers, T. H. C., Seymour, R. J., & Guza, R. T. (1996). A comparison of directional buoy and fixed platform measurements of Pacific swell. *J. Atmos. Ocean Technol.*, *13*, 231–238.
- Perignon, Y., Ardhuin, F., Cathelain, M., & Robert, M. (2014). Swell dissipation by induced atmospheric shear stress. *J. Geophys. Res.*, *119*, 6622–6630. doi: 10.1002/2014JC009896
- Pettersson, H., Kahma, K. K., & Tuomi, L. (2010). Wave directions in a narrow bay. *J. Phys. Oceanogr.*, *40*, 155–169. Retrieved from <http://journals.ametsoc>

- .org/doi/pdf/10.1175/2009JP04220.1
- Peureux, C., & Ardhuin, F. (2016). Ocean bottom pressure records from the cascadia array and short surface gravity waves. *J. Geophys. Res.*, *121*, 2862–2873. doi: 10.1002/2015JC011580
- Peureux, C., Ardhuin, F., & Guimaraes, P. V. (2021). On the unsteady steepening of short gravity waves near the crests of longer waves in the absence of generation or dissipation. *J. Geophys. Res.*, *126*. doi: 10.1029/2020JC016735
- Peureux, C., Benetazzo, A., & Ardhuin, F. (2018). Note on the directional properties of meter-scale gravity waves. *Ocean Science*, *14*, 41–52. doi: 10.5194/os-14-41-2018
- Phillips, O. M. (1958). The equilibrium range in the spectrum of wind-generated waves. *J. Fluid Mech.*, *4*, 426–433.
- Phillips, O. M. (1984). On the response of short ocean wave components at a fixed wavenumber to ocean current variations. *J. Phys. Oceanogr.*, *14*, 1425–1433. Retrieved from <https://journals.ametsoc.org/doi/abs/10.1175/1520-0485%281984%29014%3C1425%3AOTROS0%3E2.0.CO%3B2> doi: 10.1175/1520-0485(1984)014<1425:OTROS0>2.0.CO;2
- Phillips, O. M. (1985). Spectral and statistical properties of the equilibrium range in wind-generated gravity waves. *J. Fluid Mech.*, *156*, 505–531.
- Romero, L. (2019). Distribution of surface wave breaking fronts. *Geophys. Res. Lett.*, *46*, 10463–10474. doi: 10.1029/2019GL083408
- Romero, L., & Lubana, K. (2022). On the bimodality of the wind-wave spectrum: Mean-squared-slopes and azimuthal overlap integral. *J. Phys. Oceanogr.*, *52*, 1549–1562. doi: 10.1175/JPO-D-21-0299.1
- Romero, L., & Melville, K. W. (2010). Airborne observations of fetch-limited waves in the gulf of tehuatepec. *J. Phys. Oceanogr.*, *40*, 441–465.
- Ryabkova, M., Karaev, V., Guo, J., & Titchenko, Y. (2019). A review of wavespectrum models as applied to the problem of radar probing of the sea surface. *J. Geophys. Res.*, *124*, 71047134. doi: 10.1029/2018JC014804
- Soloviev, A. V., Lukas, R., Donelan, M. A., Haus, B. K., & Ginis, I. (2014). The air-sea interface and surface stress under tropical cyclones. *Scientific Reports*, *4*, 5306. doi: 10.1038/srep05306
- Stopa, J. E., Ardhuin, F., & Girard-Ardhuin, F. (2016). Wave climate in the Arctic 1992-2014: seasonality and trends. *The Cryosphere*, *10*, 1605–1629. doi: 10.5194/tc-10-1605-2016
- Sutherland, P., & Melville, W. K. (2013). Field measurements and scaling of ocean surface wave-breaking statistics. *Geophys. Res. Lett.*, *40*, 3074–3079. doi: 10.1002/grl.50584
- Sutherland, P., & Melville, W. K. (2015). Field measurements of surface and near-surface turbulence in the presence of breaking waves. *J. Phys. Oceanogr.*, *45*, 943–965. doi: 10.1175/JPO-D-14-0133.1
- Thomson, J., D’Asaro, E. A., Cronin, M. F., Rogers, W. E., Harcourt, R. R., & Shcherbina, A. (2013). Waves and the equilibrium range at ocean weather station P. *J. Geophys. Res.*, *118*, 595–5962. doi: 10.1002/2013JC008837
- Tolman, H. L., & Chalikov, D. (1996). Source terms in a third-generation wind wave model. *J. Phys. Oceanogr.*, *26*, 2497–2518. Retrieved from <http://journals.ametsoc.org/doi/pdf/10.1175/1520-0485%281996%29026%3C2497%3ASTIATG%3E2.0.CO%3B2>
- Tracy, B. A., & Resio, D. T. (1982). *Theory and calculation of the nonlinear energy transfer between sea waves in deep water* (Tech. Rep. No. 11). U.S. Army Engineer Waterways Experiment Station, Vicksburg, U.S.A.
- Tyler, G. L., Teague, C. C., Stewart, R. H., Peterson, A. M., Munk, W. H., & Joy, J. W. (1974). Wave directional spectra from synthetic aperture observations of radio scatter. *Deep Sea Res.*, *21*, 989–1016.
- van Vledder, G. P. (2006). The WRT method for the computation of non-linear

- 820 four-wave interactions in discrete spectral wave models. *Coastal Eng.*, *53*, 223–
821 242.
- 822 Webb, D. J. (1978). Nonlinear transfer between sea waves. *Deep Sea Res.*, *25*, 279–
823 298.
- 824 Young, I. R., Verhagen, L. A., & Banner, M. L. (1995). A note on the bimodal
825 directional spreading of fetch-limited wind waves. *J. Geophys. Res.*, *100*(C1),
826 773–778.
- 827 Yurovskaya, M. V., Dulov, V. A., Chapron, B., & Kudryavtsev, V. N. (2013). Di-
828 rectional short wind wave spectra derived from the sea surface photography. *J.*
829 *Geophys. Res.*, *118*, C12024. doi: 10.1002/jgrc.20296